Supporting Information

Magnitude and pathways of increased nitrous oxide emissions from uplands following permafrost thaw

Guibiao Yang[1,2], Yunfeng Peng[1], Maija E. Marushchak[3], Yongliang Chen[1], Guanqin Wang[1,2], Fei Li[1,2], Dianye Zhang[1,2], Jun Wang[1,2], Jianchun Yu[1,2], Li Liu[1,2], Shuqi Qin[1,2], Dan Kou[1,2] and Yuanhe Yang[1,2*]

1. State Key Laboratory of Vegetation and Environmental Change, Institute of Botany, Chinese Academy of Sciences, Beijing 100093, China
2. University of Chinese Academy of Sciences, Beijing 100049, China
3. Department of Environmental and Biological Sciences, University of Eastern Finland, Kuopio 70211, Finland

[*]**Corresponding author:** Dr. Yuanhe Yang, tel.: + 86 10-62836638, fax: + 86 10-62836632, E-mail: yhyang@ibcas.ac.cn

Number of pages: 11; Number of tables: 2; Number of figures: 5

Supplementary Method

Calculation of the ratio of the global warming potential (GWP) of N_2O to the GWP of CH_4 in the thermokarst and control areas

The ratio of the GWP of N_2O to the GWP of CH_4 was calculated according to the following four steps. First, we measured CH_4 flux in vegetated and exposed patches simultaneously with the measurement of N_2O flux along the thawing sequence[1]. The emissions from the control area averaged 0.026 mg N_2O m^{-2} d^{-1} and 5.04 mg CH_4 m^{-2} d^{-1}. Second, to estimate the N_2O and CH_4 flux rates in each year over the 20 years of thawing for vegetated and exposed patches, we explored the relationships of the CH_4 and N_2O fluxes with the years after collapse in vegetated and exposed patches, respectively. The CH_4 flux rate in both vegetated and exposed patches increased exponentially with the years after collapse (Figure S5a, b), whereas a negatively exponential relationship was observed between the N_2O flux and collapse years (Figure S5c, d). Due to the very high N_2O emission rates in the 1st and 2nd years obtained from the exponential relationships (Figure S5c) and the fact that this situation is unlikely to occur, we assumed that stable N_2O and CH_4 flux rates occurred for the first three years. The N_2O emission rates in the 3rd year were then used for the 1st and 2nd year calculations. Third, to further obtain weighted fluxes, we quantified the area of vegetated and exposed patches using a high-resolution topographic model of the gully generated via LiDAR (VZ-400, Riegl, Horn, Austria; analyzed with Riscan pro 2.0 software). The area fraction of exposed patches increased linearly with the years after collapse, with a corresponding linear decrease in the fraction of vegetated area (Figure S5e, f). The weighted fluxes in each year were calculated using the relative coverage of vegetated and exposed areas within this typical thermokarst

gully, which results in mean fluxes of 0.35 mg N_2O m^{-2} d^{-1} and 6.96 mg CH_4 m^{-2} d^{-1}. Finally, given that the GWP of N_2O per unit mass is 12 times higher than that of CH_4 over a 100-year time horizon[2], the GWP of N_2O emissions was calculated 59.8% of the GWP of CH_4 emissions in the thermokarst landform, whereas this fraction was only 6.2% in the control area.

Table S1 Amplification conditions, reading temperature, primer pairs, number of cycles and references used to quantify the abundance of the *nirS*, *nirK* and *nosZ* genes.

Gene	Function	Primers	Thermocycler Conditions	Number of Cycles	Reference
nirS	Nitrite reduction	*nirS*-cd3aF	94 °C for 90 s	1	Michotey et al., 2000
		nirS-R3cd	95 °C for 10 s / 56 °C for 30 s / 72 °C for 40 s	40	
nirK	Nitrite reduction	*nirK* 1F	95 °C for 30 s	1	Braker et al., 1998
		nirK 5R	95 °C for 10 s / 60 °C for 30 s / 72 °C for 20 s	40	
nosZ	Nitrous oxide reduction	*nosZ* F	94 °C for 90 s	1	Throbäck et al., 2004
		nosZ 1662R	95 °C for 10 s / 58 °C for 30 s / 72° C for 40 s	40	

Table S2 Results of repeated-measures ANOVA on the effects of the thawing stage (TS), sampling date (D) and their interactions on N_2O fluxes in the vegetated patches along the thaw sequence in 2015 and 2016, and the effects of patch types (PT), sampling date (D) and their interactions on N_2O fluxes at the early stage and 2016.

Year	2015			2016					
Source	TS	D	TS×D	TS	D	TS×D	PT	D	PT×D
F	13.23	3.06	1.54	12.51	0.46	0.54	23.39	0.92	0.81
P	**<0.001**	**0.001**	0.10	**<0.001**	0.76	0.87	**<0.001**	0.46	0.53

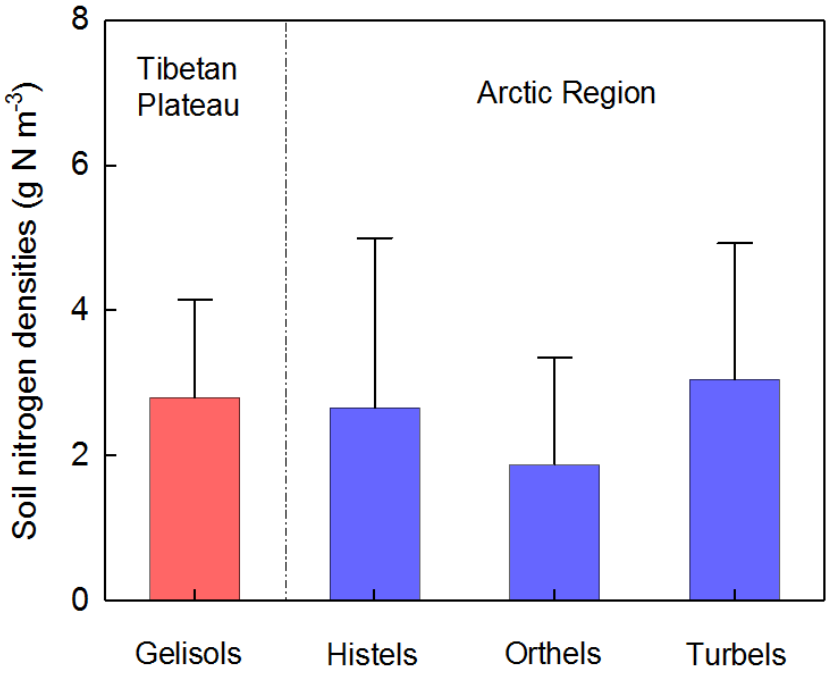

Figure S1 Comparisons of the soil nitrogen densities in the 0–100 cm (mean±SD) between Tibetan gelisols (distributed by swamp meadow) and the three different soil types across the northern circumpolar permafrost region[6].

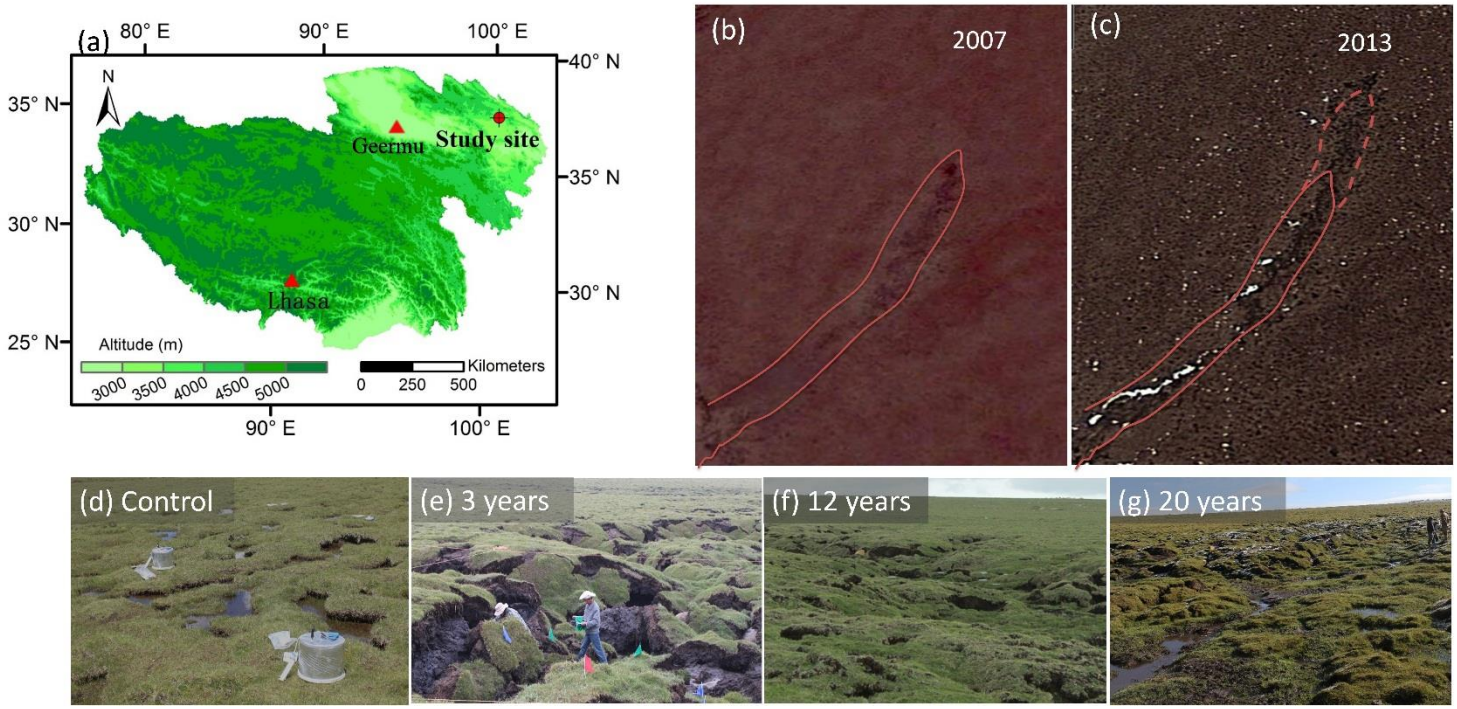

Figure S2 Location map of the study site (a); satellite images from 2007 (b) to 2013 (c); photographs of the control (d) and at 3 years (e), 12 years (f), and 20 years (g) since the collapse.

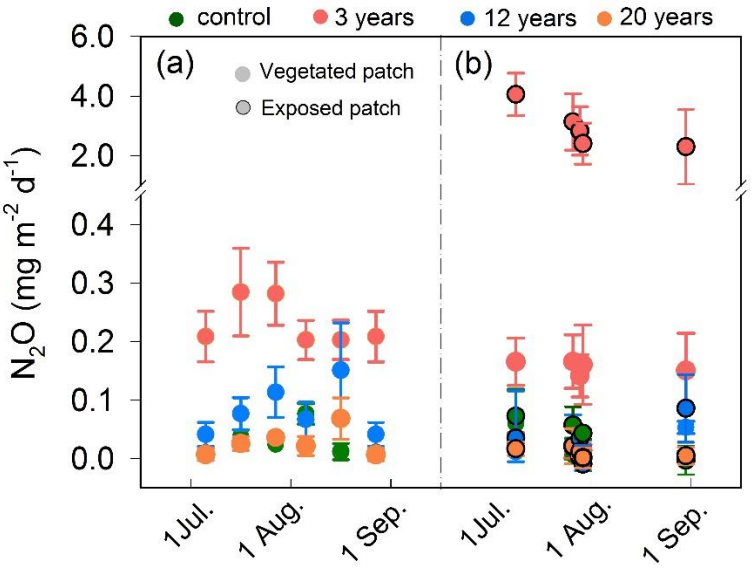

Figure S3 Seasonal dynamics of N_2O fluxes in the vegetated patches in 2015 (a) and in the vegetated and exposed patches in 2016 (b) along the thaw sequence. Error bars represent the standard error (n=10).

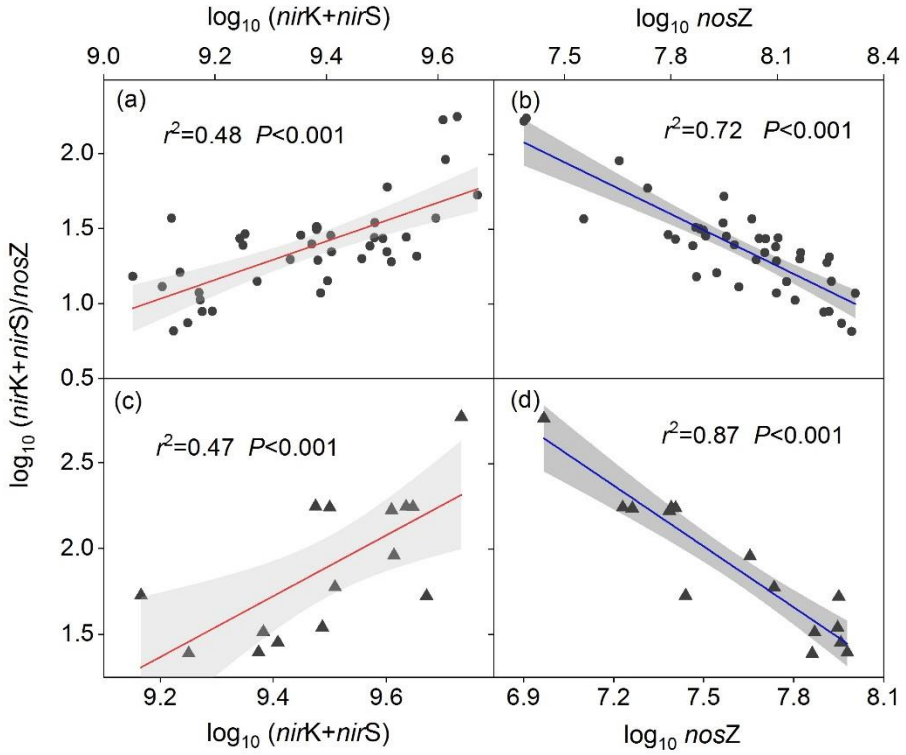

Figure S4 The relationship of (*nirK*+*nirS*)/*nosZ* with *nirS*+*nirK* (a, c) and *nosZ* (b, d) in the vegetated and exposed soil patches. The solid line is the regression curve, and the gray area indicates the 95% confidence interval. The statistics (r^2 and *P* values) for the linear regression are shown.

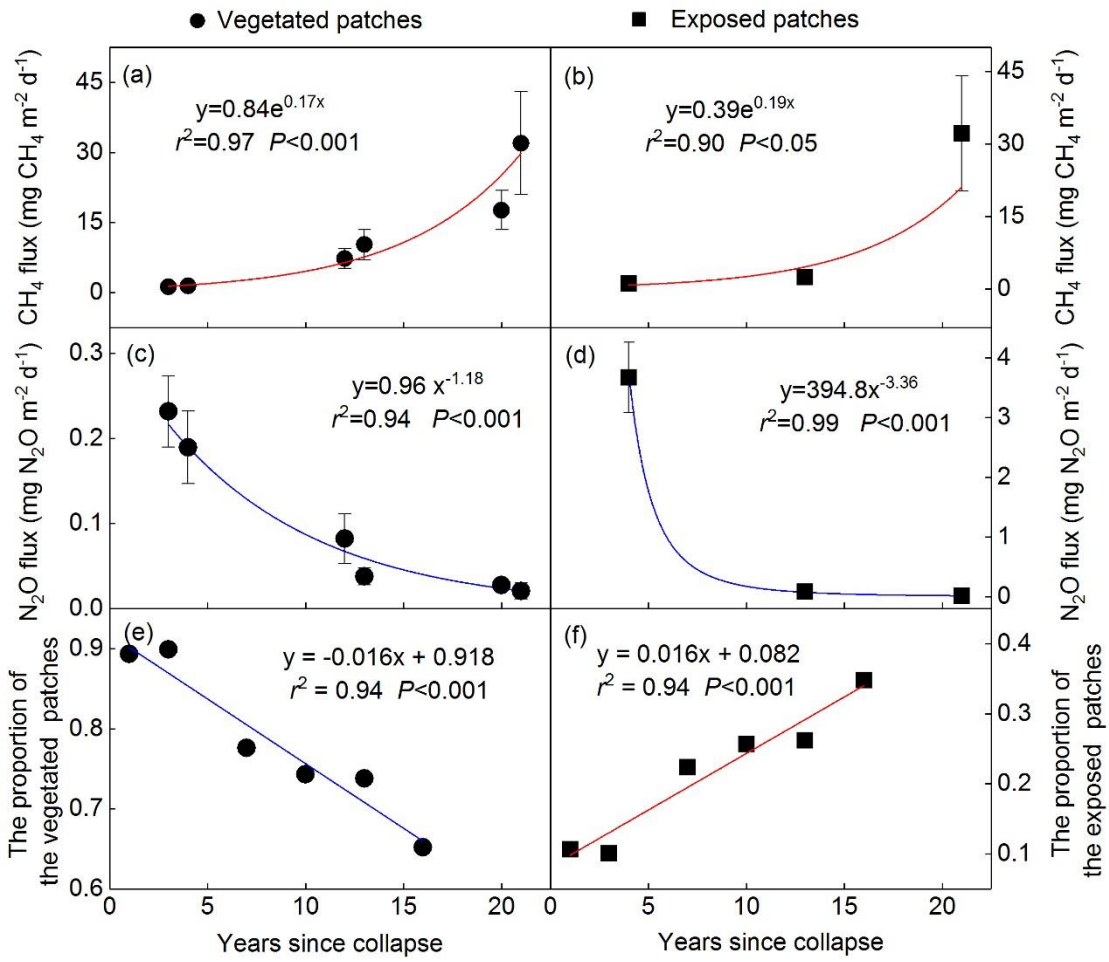

Figure S5 Changes in CH_4 and N_2O fluxes in the vegetated (a, c) and exposed soil patches (b, d), and the area proportion of the vegetated (e) and exposed soil patches (f) with time since permafrost collapse in a typical thermos-erosion gully on the Tibetan Plateau.

References

(1) Yang, G.; Peng, Y.; Olefeldt, D.; Chen, Y.; Wang, G.; Li, F.; Zhang, D.; Wang, J.; Yu, J.; Liu, L.; *et al.* Changes in methane flux along a permafrost thaw sequence on the Tibetan Plateau. *Environ Sci Technol* **2017** *52*, (3), 1244–1252.

(2) IPCC *Climate Change 2013: The Physical Science Basis. Contribution of Working Group I to the Fifth Assessment Report of the Intergovernmental Panel on Climate Change*. Cambridge University Press: Cambridge. 2013.

(3) Braker, G.; Fesefeldt, A.; Witzel, K. P.; Braker, G.; Fesefeldt, A.; Witzel, K. P. Development of PCR primer systems for amplification of nitrite reductase genes (*nir*K and *nir*S) to detect denitrifying bacteria in environmental samples. *Appl Environ Microb,* **1998** *64*, (10), 3769-3775.

(4) Michotey V.; Méjean V.; Bonin P. Comparison of methods for quantification of cytochrome cd1-denitrifying bacteria in environmental marine samples. *Appl Environ Microb,* **2000** *66*, (4), 1564-1571.

(5) Throback I.N.; Enwall K.; Jarvis A., Hallin S. Reassessing PCR primers targeting nirS, nirK and nosZ genes for community surveys of denitrifying bacteria with DGGE. *FEMS Microbiol Ecol,* **2004** *49*, (3), 401-417.

(6) Harden J.W.; Koven C.D.; Ping C.L. Field information links permafrost carbon to physical vulnerabilities of thawing. *Geophys Res Lett*, **2012** *39*, (15), 51-60.